Article

Not peer-reviewed version

On the Unique Morphology and Elastic Properties of Multi-jet Electrospun Cashew Gum-Based Fiber Mats

Mattia Grumi , Cristina Prieto * , Roselayne Ferro Furtado , H. N. Cheng , Atanu Biswas , Sara Limbo , Luís Cabedo , Jose M. Lagaron *

Posted Date: 17 March 2024

doi: 10.20944/preprints202403.0865.v1

Keywords: cashew gum; nanofibers; electrospinning

Article

On the Unique Morphology and Elastic Properties of Multi-jet Electrospun Cashew Gum-based Fiber Mats

Mattia Grumi [1], Cristina Prieto [1,*], Roselayne F. Furtado [2], H.N. Cheng [3], Atanu Biswas [4], Sara Limbo [5], Luis Cabedo [6] and Jose M. Lagaron [1,*]

[1] Novel Materials and Nanotechnology Group, Institute of Agrochemistry and Food Technology (IATA), Spanish Council for Scientific Research (CSIC), Calle Catedrático Agustín Escardino Benlloch 7, 46980 Paterna, Spain.
[2] Embrapa Agroindústria Tropical, Rua Dra. Sara Mesquita 2270, CEP 60511-110, Fortaleza, CE, Brazil
[3] (Retired) U.S. Department of Agriculture, Agriculture Research Service, Southern Regional Research Center, 1100 Allen Toussaint Blvd., New Orleans, LA, 70124, USA
[4] U.S. Department of Agriculture, Agricultural Research Service, National Center for Agricultural Utilization Research, 1815 N. University St, Peoria, IL, 61604, USA
[5] Department of Food, Environmental and Nutritional Sciences (DeFENS), Università degli Studi di Milano, via Giovanni Celoria 2, 20133, Milan, Italy
[6] Polymers and Advanced Materials Group (PIMA), Universitat Jaume I (UJI), Castellón, Spain
* Correspondence: cprieto@iata.csic.es (C.P.); lagaron@iata.csic.es (J.M.L.)

Abstract: This study investigates the unique morphology and mechanical properties of multi-jet electrospun cashew gum (CG) when combined with high molecular weight polyethylene oxide (PEO) and glycerol. Cashew gum (CG) is an inexpensive, non-toxic polysaccharide derived from Anacardium occidentale trees. Initially, the electrospinnability of aqueous solutions of cashew gum alone or in combination with PEO was evaluated. It was found that cashew gum alone was not suitable for electrospinning; thus, adding a small quantity of PEO was needed to create the necessary molecular entanglements for fiber formation. By using a single emitter with a CG:PEO ratio of 85:15, straight and smooth fibers with some defects were obtained. However, additional purification of the cashew gum solution and the incorporation of glycerol as a plasticizer were necessary to produce defect-free straight and smooth fibers. Interestingly, when the optimized formulation was electrospun using multiple simultaneous emitters, thicker aligned fiber bundles were achieved. Moreover, the resulting oriented fiber mats exhibited unexpectedly high elongation at break at ambient conditions. These findings highlight the potential of this bio-polysaccharide-based formulation for non-direct water contact applications requiring elastic properties.

Keywords: cashew gum; nanofibers; electrospinning

1. Introduction

Plastic pollution and lack of biodegradability, together with the scarcity of oil sources, have prompted worldwide research seeking biodegradable and renewable alternatives to petroleum-based polymers for various applications [1–3]. In this connection, agro-based polymers and natural gums stand out as promising biodegradable polymeric materials [4]. The term "gum" refers to polysaccharide hydrocolloids, which are not part of the vegetable cell wall, but are exudates or slims [5]. The low cost, low risk of side effects, biocompatibility, and their environmentally friendly processing are among the advantages attributed to natural gums [6,7].

Cashew gum is a complex water-soluble heteropolysaccharide extracted from the bark epithelial cells of *Anacardium occidentale Linn* trees, commonly known as the cashew trees [8]. These trees are mainly located in tropical and subtropical countries, even though their cultivation is, up to now, mostly aimed at the production of cashew nuts, while cashew gum was traditionally considered a low-value by-product [9]. Cashew gum can be obtained by natural exudation, since it is synthetized

 doi:10.20944/preprints202403.0865.v1

in the epithelial cells and secreted into ducts through the cashew tree bark as a response to mechanical stimuli or attacks by pathogens [7,10], or it can be obtained by means of incisions on the trunk and branches of the tree. The extraction can also be promoted by the use of chemical stimulants [11]. Cashew gum structure is characterized by a highly-branched galactan framework consisting of chain of ß-(1-3)-linked D-galactose residues branched and interspaced with ß-(1-6) linkages [12,13], in which the main residues are represented by galactose (59.4-73 %), glucose (6.4-14 %), arabinose (4.2-5.3 %), rhamnose (2.4-4 %) and glucuronic acid (6.3-13.5 %) [14,15]. Among the potential applications of cashew gum, several studies have been conducted revealing its huge potential in different sectors such as food, pharma, and food packaging, among others [16,17]. Moreover, it can be asserted that cashew gum is an inexpensive, non-toxic, biocompatible, biodegradable natural polymer with good rheological and mechanical properties [15–17], readily soluble in water, and with interesting emulsifying, adhesive, and stabilizing properties [11,18]. Cashew gum has also functional properties such as mucoadhesion, anti-inflammatory, anti-microbial, anti-diarrheal, anti-tumoral and hypoglycemic effects [17]. All these properties suggest that cashew gum is a suitable candidate for multiple purposes such as food, pharma, biomedicine, cosmetics, agriculture, or food packaging applications.

Among the available processing technologies during the last two decades, a growing interest has been focused on the novel electrohydrodynamic processing technology (EHDP) that has emerged as a versatile and simple approach for the manufacturing of ultrathin (micron and submicron) polymer structures with highly specific surface areas and porosities for a wide variety of industrial applications, including food packaging production [19–21]. During the electrospinning process, a polymeric solution is exposed to a high electric field, which is able to overcome the surface tension of the solution enabling a charged fluid stream of the polymeric phase to be ejected towards the collector [22]. During the flight time, the solvent is evaporated at room temperature and the jet undergoes continuous elongation allowing the creation of widely interconnected micro- or nanofibers that form a three-dimensional network of the non-woven mat [23,24]. These micro and nanostructures offer many functional advantages, such as superior mechanical properties, flexibility, large surface-to-mass ratio, tailored morphology, tunable porosity and the capability of encapsulation and subsequent release of active and bioactive compounds [17,21,25–29]. Therefore, the electrospinning technology is very promising for the creation of mono- or interlayers or coatings with enhanced flexibility and transparency, while potentially retaining the barrier performance with respect to gases and vapors of conventionally produced films [17,30–34].

The objective of this study was the development and characterization of electrospun fibers based on cashew gum. Cashew gum was previously studied by Vázquez-González et al. [17], who assessed the electrosprayability of cashew gum to form capsules. On the other hand, Andrade et al. [11] studied the thermoplastic extrusion of cashew gum in order to assess the effect of this processing technique on this natural gum. Furthermore, Oliveira et al. and Silva et al. [10,35] studied the formation of cashew gum-based films by casting or by blending the biopolymer with gelatin or nanofibrillated bacterial cellulose. Recently, de Souza et al. [36] successfully blended cashew gum with alginate, galactomannans, and gelatin in order to produce edible coatings for food preservation.

In this work, the electrospinning of cashew gum combined with high molecular weight PEO and glycerol was first performed and their unique morphological and mechanical properties characterized. The developed formulation showed an unexpected elasticity during tensile tests potentially representing a sustainable alternative to conventional non-biobased elastomers.

2. Materials and Methods

2.1. Materials

Non-purified cashew gum (*Mw*: 2.13 x 10^4 Da) was collected from native *Anacardium occidentale L.* trees cultivated in the experimental field of Embrapa Tropical Agroindustry (Fortaleza, CE, Brazil), and polysaccharide isolation from cashew gum (CG) was performed following the methodology previously described by da Silva et al. [37]. Polyethylene oxide (PEO) (*Mw*: between 6.0 x 10^5 Da to

 doi:10.20944/preprints202403.0865.v1

5.0 x 10^6 Da) and Span® 20 surfactant were purchased from Sigma Aldrich (St. Louis, MO, USA). Pure glycerol (*Mw*: 9.21 x 10^1 Da) was provided by Panreac AppliChem (Barcelona, Spain). Distilled water was used as the only solvent throughout this study. All chemicals were used without further purification.

2.2. Preparation of Polymeric Solutions

For the evaluation of the electrospinnability of CG, different formulations of CG in distilled water were prepared, as shown in Table 1. CG was first dissolved at a concentration of 120% (w/v) in distilled water for 48 h at room temperature, under magnetic stirring, and Span® 20 was used as a surfactant at a concentration of 3% (w/v). This corresponds to solution *S0*.

For the purpose of improved fiber formation, blending with a higher molecular weight supporting polymer was considered. In this case, blending with PEO of different molecular weights was proposed. Total solid concentration in solution (TCS) varied from 50% to 15% (w/v). The CG: PEO ratio varied from 95:5 to 82:18. For the preparation of the solutions, CG was first dissolved in distilled water for 48 h at room temperature under magnetic stirring. Then, PEO was added to the cashew gum solution, which was further stirred for at least 3 h. In all cases, Span® 20 was added to the solution at 1% (w/v) with respect to the volume of distilled water used (solutions *S1-S8*).

In further tests, the removal of some impurities in cashew gum was undertaken to improve the stability of the electrospinning process. Thus, two consecutive centrifuging steps were conducted after the complete solubilization of CG in distilled water. Each centrifuging step was performed for 20 min at 11,872 g using a J-26 XPI Beckman Avanti equipment with a JA-25.50 rotor (Beckman Coulter Life Sciences, Indianapolis, IN, USA). The supernatant without impurities was recovered and PEO was added to the solution. Then, Span® 20 was added as a surfactant to the solution at 1% (w/v) with respect to the volume of distilled water. The obtained solution was gently homogenized under magnetic stirring at 35 °C for 4 h (solution *S9*). In this solution, a final CG: PEO ratio of 82:18 was achieved.

For three formulations, a plasticizer, in this case glycerol, was used at concentrations of 1.5-3.5 % (w/v). Glycerol was added to the CG solution, after the addition of PEO, and it was further stirred for at least 3 h in order to guarantee homogeneity (solutions *S10-S12*).

Three different polymeric solutions were additionally prepared and used as controls in order to better understand the specific morphology and properties of the multi-jet electrospun *S12* optimal blend. Details of the composition of these solutions, *Control_1* to *Control_3*, are gathered in Table 1.

Table 1. Composition of the cashew gum (CG) solutions prepared for the electrospinning process. TCS is the total concentration of solids solubilized in 100 mL of distilled water; CG:PEO ratio refers to the weight ratio of the two polymers included in the TCS; and CG loss after centrifuging refers to the percentage of cashew gum, in the form of impurities, removed through the centrifugation process.

Solution	TCS (% w/v)	CG:PEO Ratio	PEO *Mw* (Da)	Span® 20 (% w/v)	Glycerol (% w/w)	CG loss after centrifuging (% w/v)
S0	120	100:0	-	3.00	-	-
S1	50	95:5	6 x 10^5	1.00	-	-
S2	50	90:10	1 x 10^6	1.00	-	-
S3	20	95:5	5 x 10^6	1.00	-	-
S4	20	90:10	5 x 10^6	1.00	-	-
S5	20	85:15	5 x 10^6	1.00	-	-
S6	15	95:5	5 x 10^6	1.00	-	-
S7	15	90:10	5 x 10^6	1.00	-	-
S8	15	85:15	5 x 10^6	1.00	-	-
S9	15	82:18	5 x 10^6	1.00	-	< 2.30
S10	15	82:18	5 x 10^6	1.00	1.5	< 2.30

 doi:10.20944/preprints202403.0865.v1

S11	15	82:18	5 x 10^6	1.00	2.5	< 2.30
S12	15	82:18	5 x 10^6	1.00	3.5	< 2.30
Control_1	15	82:18	5 x 10^6	1.00	-	< 2.30
Control_2	2.7	0:100	5 x 10^6	1.00	-	-
Control_3	2.7	0:100	5 x 10^6	1.00	3.5	-

2.3. Physicochemical Characterization of the Solutions

Prior to electrospinning, the solutions were characterized in terms of their viscosity, electrical conductivity, and surface tension. The solution viscosity was determined using a rotational viscosimeter, ROTAVISC lo-vi control (IKA-Werke GmbH & Co. KG; Staufen, Germany) equipped with a "sp-2" spindle rotating at 1.0 rpm. The electrical conductivity was analyzed with a multi-parameter potentiometer, Hanna Instruments HI-4521 (Melrose, MA, USA). The surface tension was measured in an EasyDyne tensiometer K20-model (Krüss GmbH, Hamburg, Germany), using the Wilhelmy Plate method. All measurements were carried out in triplicate at room temperature.

2.4. Electrospinning Process

The electrospinning process was carried out using a Fluidnatek® LE-50 equipment (Bioinicia S.L., Valencia, Spain). The prepared solutions were drawn in a plastic syringe that was placed in a syringe pump and connected by a polytetrafluoroethylene (PTFE) tube to a single injector linked to a stainless-steel needle. A positive electrode at a high voltage was coupled to the collector. Different operational parameters, viz., voltage, distance between injector and collector, flowrate, needle gauge, were tested in order to optimize fibers production. The applied flowrate ranged from 50 to 450 μL/h. The tip-to-collector distance was increased from 17 to 30 cm. The applied positive voltage ranged from +17 to +31 kV. Besides, the applied negative voltage was always set at -9 kV, when it was required. The needle gauge used was in the range between 22 and 27. All the trials performed to attain optimal fibers were made at 25 °C and 40% relative humidity (RH).

Besides the above single-needle experiments, the selected *S12* sample as well as *Control_1* - *Control_3* were produced in a higher throughput mode using a Fluidnatek® LE-100 equipment (Bioinicia S.L., Valencia, Spain) to obtain a wider homogeneous sample area to test for mechanical properties. In this case, the positive and negative voltage were optimally set at +15 and -20 kV, respectively; the tip-to-collector distance was set at 24.5 cm; the flowrate was set at 1 mL/h per needle, using a 5-needle-injector (the injector setup consisted in 5 needles placed in a row with a distance between the needles of 13 mm), over a drum collector with a rotational speed of 100 rpm (collector diameter: 110 mm; linear speed: 0.58 $m \cdot s^{-1}$); the X axis scanning motion was set to cover the whole width of the drum collector (300 mm) using a motion speed of 50 mm/s. The needle gauge used was 23. This experiment was optimally conducted at 40 °C and 25% RH. All the samples were stored for at least 24 hours in a desiccator at 25 °C and a controlled 0% RH until further analysis.

2.5. Characterization of the Electrospun Fibers

2.5.1. Scanning Electron Microscopy (SEM)

The morphology of the electrospun fibers was analyzed by scanning electron microscopy (SEM), using a Hitachi S-4800 microscope (Hitachi High-Technologies Corporation, Tokyo, Japan). Each sample, sized approximatively 5 mm x 5 mm, was affixed with double-side tape on the SEM sample holder. Prior to analysis, all the samples were coated with a gold/palladium alloy for 2 min using a Polaron sputter coater (Quarum Technologies, Kent, UK). During the SEM analyses, an electron beam acceleration of 10 kV was applied. Average fibers diameter was determined using the software ImageJ bundled with Zulu OpenJDK Version 13.0.6 (National Institute of Health, Bethesda, MD, USA), from the measurement of at least 50 fibers.

 doi:10.20944/preprints202403.0865.v1

2.5.2. Thermogravimetric Analysis (TGA)

For the assessment of the thermal stability of PEO, cashew gum, and the electrospun cashew gum/PEO-based fibers obtained from *S12*, TGA was performed under nitrogen atmosphere in a 550-TA thermogravimetric analyzer (TA Instruments, New Castle, DE, USA). All TGA tests were performed in triplicate. TGA curves were obtained after conditioning the samples placed in the sensor at 30 °C for 5 minutes. After that, the samples were heated from 30 °C to 600 °C at a rate of 10 °C/ minute. Derivative TGA curves (DTG), obtained using TA analysis software TRIOS, Version 5.1 (TA Instruments, New Castle, DE, USA), expressed the weight loss rate as a function of temperature.

2.5.3. Differential Scanning Calorimetry (DSC)

Thermal transitions of PEO and CG powder as well as those of the electrospun CG/PEO-based fibers obtained from *S12* were analyzed using a DSC-8000 analyzer (PerkinElmer Inc., Waltham, MA, USA) equipped with a cooling accessory Intracooler 2 (PerkinElmer Inc., Waltham, MA, USA). Approximately, 3 mg of sample were placed into a hermetically sealed aluminum pan, while an empty pan was used as a reference. Calibration was previously conducted using an indium sample. The samples were first heated from 30 °C to 175 °C, then cooled back to 0 °C, and then heated back again up to 245 °C. The heating and cooling rates were set at 10 °C/ min. The experiments were conducted under nitrogen atmosphere and all DSC tests were performed in triplicate. The values of the melting temperature (T_m) and enthalpy of melting (ΔH_m) were obtained from the heating scans, while the crystallization temperature from the melt (T_c) and enthalpy of crystallization (ΔH_c) were extracted from the cooling scans.

2.5.4. Wide-Angle X-ray Scattering (WAXS)

The crystallographic structural analysis of PEO, CG, and the electrospun CG/PEO-based fibers obtained from *S12*, was performed by WAXS in a WAXS D4-Model Endeavor diffractometer (Bruker Corporation, Ettlingen, Germany), following the same protocol previously reported by Vázquez-González et al. [17] The samples were scanned at scattering angles (2θ) between 5 and 30°, at room temperature, in reflection mode, applying incident Cu K-alpha radiation (Cu Kα = 1.54 Å). The generator was running with an operating voltage of 40 kV and a filament current of 40 mA.

2.5.5. Mechanical Tests

Tensile tests of electrospun fibers from *S12*, *Control_2* fibers, and *Control_3* fibers were performed in accordance with the ASTM standard method D638 using an AGS-X 5000N universal testing machine (Shimadzu Corporation, Kyoto, Japan) equipped with a 500 N load cell. Dumb-bell shape samples were die-cut from the fiber mat in the direction of rotation of the drum collector and also in the perpendicular direction. The tests were carried out under room conditions, i.e. 25 °C and 45% RH, at a crosshead rate of 10 mm/min. Samples were conditioned to the test conditions for 24 hours prior to the tensile assay. A minimum of six specimens were measured for each sample.

2.5.6. Statistical Analysis

Each treatment was carried out in triplicate and the results of the properties were evaluated with a 95% significance level ($p \leq 0.05$). Analysis of variance (ANOVA) and multiple comparison test (Tukey test) were conducted to identify significant differences among the treatments. To this end, the software Origin Pro, Version 2022 (OriginLab Corporation, Northampton, MA, USA) was used.

3. Results and Discussion

3.1. Fiber Production and Physicochemical Characterization of the Solutions

The ability of CG to form fibers via electrospinning was first evaluated alone and also in combination with different mass ratios of higher molecular weight supporting polymers such as

 doi:10.20944/preprints202403.0865.v1

polyethylene oxide (PEO). In the latter case, the objective was to obtain cashew gum fibers with the smallest amount of PEO possible. Prior to electrospinning, viscosity, electrical conductivity, and surface tension of the solutions were assessed in order to anticipate the stability of the electrospinning process. Table 2 displays the characterization of the solutions with the best electrospinning performance. Solution *S8*, which was made by CG and PEO_{5M} solubilized in distilled water, showed a viscosity of 24,647 ± 148 cP, whereas solution *S9* presented a viscosity value of 21,849 ± 197 cP, which was significantly lower than the viscosity value obtained for solution *S8*. This decrease in the viscosity value could be due to the removal of insolubilized GC particles during the centrifuging process, which were present in solution *S8*. Similar observations, in terms of viscosity reduction were reported earlier [34] when purifying polymeric solutions based on unpurified PHBV by centrifugation. However, an increase in solution viscosity was observed for solution *S12*, which showed a viscosity of 24,189 ± 115 cP, as a consequence of the addition of a 3.5% w/w of glycerol. This effect was previously described by Akinalan Balik et al. when studying the electrospinnability of pectin due to the addition of glycerol [38]. The latter authors observed an increase in viscosity even using a lower quantity of glycerol, i.e., 3 % wt.

Table 2. Physico-chemical properties of solutions of CG:PEO (*S8*), CG:PEO centrifuged (*S9*), and CG:PEO with 3.5% w/w of glycerol and also centrifuged (*S12*).

Sample	Viscosity (cP)	Conductivity (μS/cm)	Surface Tension (mN/m)
S8	$24{,}647 \pm 148^{a}$	815.1 ± 0.00^{b}	36.0 ± 0.6^{b}
S9	$21{,}849 \pm 197^{b}$	657.1 ± 0.03^{a}	39.4 ± 1.1^{a}
S12	$24{,}189 \pm 115^{c}$	645.4 ± 0.00^{c}	$37.0 \pm 1.2^{a,b}$

*Each column represents the mean value ± standard deviation of three independent replicas. Different letters in the same column indicate a significant difference among the samples ($p < 0.05$).

As regards conductivity, solution *S8* presented the highest conductivity. The reduction of the conductivity value observed in solution *S9* and *S12* may be ascribed to the removal of some salts and ions by centrifuging the solubilized cashew gum, which facilitate a more stable electrospinning process since solutions with high electrical conductivity values often suffer from process instability [39].

In terms of surface tension, it is important to indicate that the addition of Span® 20 was required for all the solutions in order to decrease the surface tension value and get a stable electrospinning process. Since the solvent used was distilled water, which is featured by a high surface tension value (around 70 mN/m) [40], the addition of a surfactant, such as Span® 20 allowed a surface tension reduction down to values adequate for a good electrospinning process (around 40 mN/m) [41,42]. In view that the surfactant concentration was about the same (1% w/v) in these solutions, no significant differences were observed between these three samples.

3.2. Morphology of Electrospun CG-PEO Fibers

The electrospinning of the neat CG solution (solution *S0*) did not result in the production of consistent fibers. Thick structures were collected instead, as can be seen from Figure 1S included in the Supplementary Materials.

All the prepared CG-PEO solutions were intended to find the minimum amount of supporting polymer required to generate the molecular entanglements necessary to obtain the desired electrospun fibers. However, solution *S5* was found not to be electrospinnable, due to its excessively high viscosity [43], and hence it could not be processed and was excluded from the study. On the other hand, it was possible to electrospin solutions *S1*, *S2*, *S3*, *S4*, *S6*, *S7*, *S8*, *S9*, *S10*, *S11*, and *S12*, and their optimal processing conditions were summarized in Table 3.

 doi:10.20944/preprints202403.0865.v1

Table 3. Electrospinning optimized conditions to obtain CG-based fibers with good morphology. As for voltage, the values of, respectively, positive, and negative voltage conditions used are reported.

Solution	Voltage (V+/V-) (kV)	Flowrate (μL/h)	Tip-to-collector distance (cm)	Needle Gauge	Fiber formation
S0	+15/ -0	250	12.0	27	no
S1	+25/ -9	800	20.0	22	no
S2	+31/ -0	500	20.0	22	no
S3	+29/ -9	300	28.0	23	yes
S4	+29/ -9	200	22.0	23	yes
S5	//	//	//	//	no
S6	+29/ -9	400	28.0	25	no
S7	+29/ -9	300	28.0	23	yes
S8	+29/ -9	300	20.5	23	yes
S9	+22/ -9	450	20.0	22	yes
S10	+22/ -9	450	28.5	22	yes
S11	+22/ -9	450	28.5	22	yes
S12	+22/ -9	450	30.0	22	yes

Figure 1 shows the micrographs of the electrospun fibers obtained from solutions *S1* and *S2*, having a total concentration of solids of 50% w/v, and being produced with PEO molecular weights of $6 \cdot 10^5$ and $1 \cdot 10^6$ Da. The solution *S1*, as it can be appreciated from Figure 1, led to the production of beaded fibers. Similar result was obtained with solution *S2*. For this reason, it was decided to use a higher molecular weight PEO and to decrease the total concentration of solids up to a value of 20% w/v.

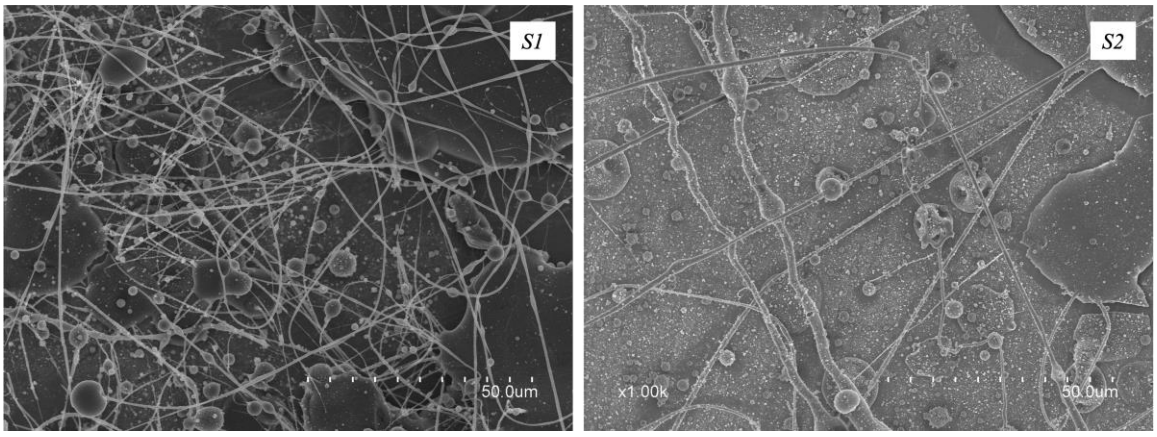

Figure 1. SEM micrographs of the electrospun fibers obtained from solutions *S1* and *S2*.

In solutions *S3*, *S4*, and *S5*, PEO with a molecular weight of 5 $x10^6$ Da (PEO_{5M}) was used and the total solid concentration was decreased to 20% w/v. The experimented CG:PEO ratios were 95:5, 90:10, and 85:15, respectively. Solution *S3* allowed the production of fibers with a better morphology compared to those obtained from solution *S1*, as it can be appreciated from observation of Figure 2, but still presented a considerable number of beads. The beads formation could be related to the viscoelastic properties of the solution, as well as to the processing conditions [44]. By increasing the ratio of PEO (solution *S4)*, more homogeneous fibers were obtained, compared to those obtained with solution *S3*, even if some wet fibers were seen, probably due to processing instabilities from the presence of some impurities. As previously reported, it was not possible to electrospun solution *S5*, probably due to its high content of PEO_{5M} that generated excessive viscosity.

 doi:10.20944/preprints202403.0865.v1

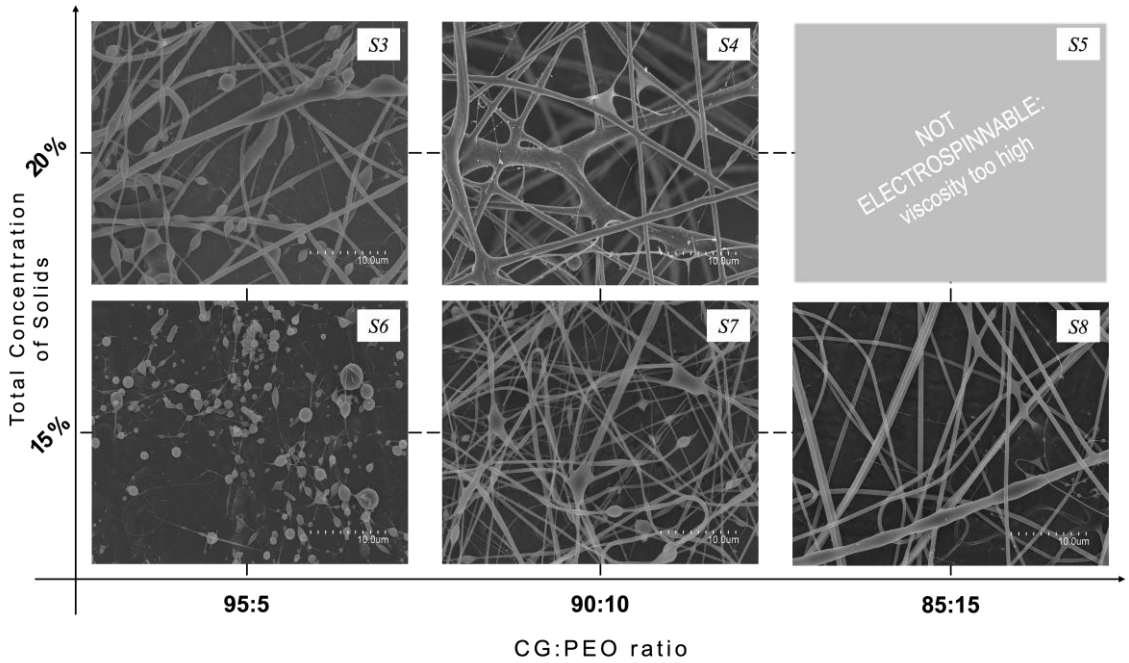

Figure 2. SEM micrographs of the electrospun fibers obtained from solutions *S3-S8*.

Additionally, a lower total solid concentration of 15% w/v was explored, with CG:PEO_{5M} ratios of 95:5, 90:10, and 85:15, respectively, being identified as solutions *S6*, *S7* and *S8*. Solution *S6* did not result in the production of fibers, as it can be observed from Figure 2, and only particles were produced. Increasing the PEO_{5M} content allowed the production of fibers but still showed some spindle-like defects and wet fibers were also collected. The ratio CG:PEO_{5M} of 85:15 (Solution *S8*), on the contrary, allowed the formation of smooth fibers almost defect-free as shown in Figure 2. The average diameter of these fibers was 0.9 ± 0.2 µm.

In the effort to improve the morphology further, a centrifuging step after CG solubilization was performed to remove some CG impurities (solution *S9*). As shown in Figure 3, this strategy allowed the production of fiber mats with an enhanced morphology and completely free of defects. However, the fiber mats obtained were deemed too fragile to be handled. For this reason, the addition of a plasticizer, such as glycerol, was considered. Furthermore, Figure 3 showed how the different amounts of glycerol, added in the centrifuged CG:PEO_{5M} solution, affected the electrospun fibers morphology. Solutions *S10* to *S12* were related to fibers containing 1.5%, 2.5%, and 3.5% w/w of glycerol, respectively. The use of the plasticizer let to the production of defect-free electrospun fibers with enhanced morphology. Similar observations were reported earlier [38] when studying the electrospinnability of pectin using also glycerol as a plasticizer. Solution *S12* was chosen as the optimal formulation, namely the solution that led to produce the best fibers in terms of morphology, but also in terms of reduced fragility, especially when compared to the fibers obtained from solutions *S8* and *S9*, and any further post-treatment would not be needed. Further studies will continue to be focused on this formulation. Fibers obtained with solution *S12* presented an average fiber diameter of 3.1 ± 1.0 µm. The increase in fiber diameter observed in comparison with fibers obtained from solution *S8* could be due to the increase in viscosity produced as a consequence of the centrifugation process and the addition of glycerol, as reported before. Similar results were observed by Melendez-Rodriguez et al. [34] who observed a significant increase in the diameter of the unpurified PHBV-based fibers after a centrifuging step, suggesting a clear improvement of the polymer purity, together with an increase in the viscoelastic properties of the material processed by electrospinning, which led to the production of fibers with larger diameters [45]. In another study conducted by Akinalan et al. [38], the addition of glycerol led to the production of significantly thicker pectin-based electrospun fibers, probably due to the plasticizing effect of glycerol which favored the molecular entanglement of the polymer chains. A similar phenomenon was also reported earlier [46], where the utilization of

 doi:10.20944/preprints202403.0865.v1

glycerol resulted in electrospun fibers with larger diameters compared to those where the glycerol was not used.

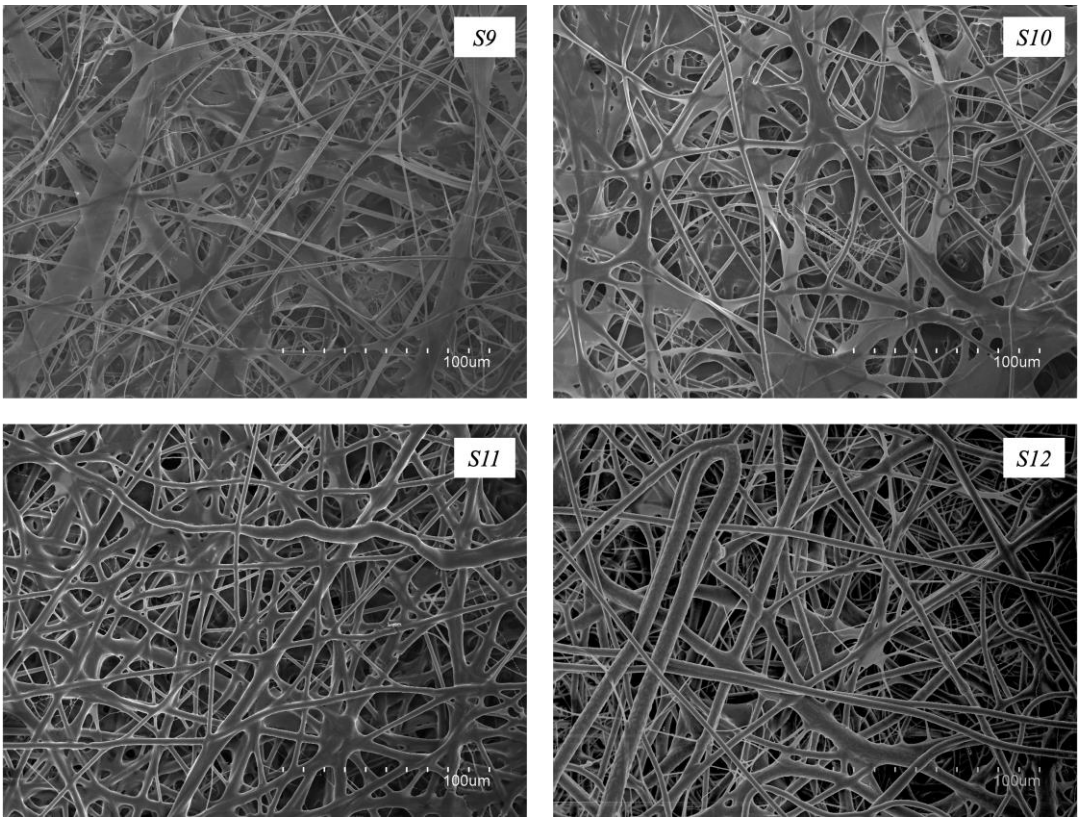

Figure 3. SEM micrographs of the electrospun fibers obtained from solutions *S9-S12*.

3.3. Thermal Properties and Thermal Stability

3.3.1. Differential Scanning Calorimetry (DSC)

Thermal transitions of electrospun fibers from solution *S12*, neat CG powder, neat PEO_{5M} powder, and pure glycerol were investigated through differential scanning calorimetry (DSC). The DSC curves are shown in Figure 4.

The DSC curve of neat CG powder did not show any melting or crystallization events in the different heating and cooling steps, which may be related to an amorphous structure of the biopolymer [38,47].

 doi:10.20944/preprints202403.0865.v1

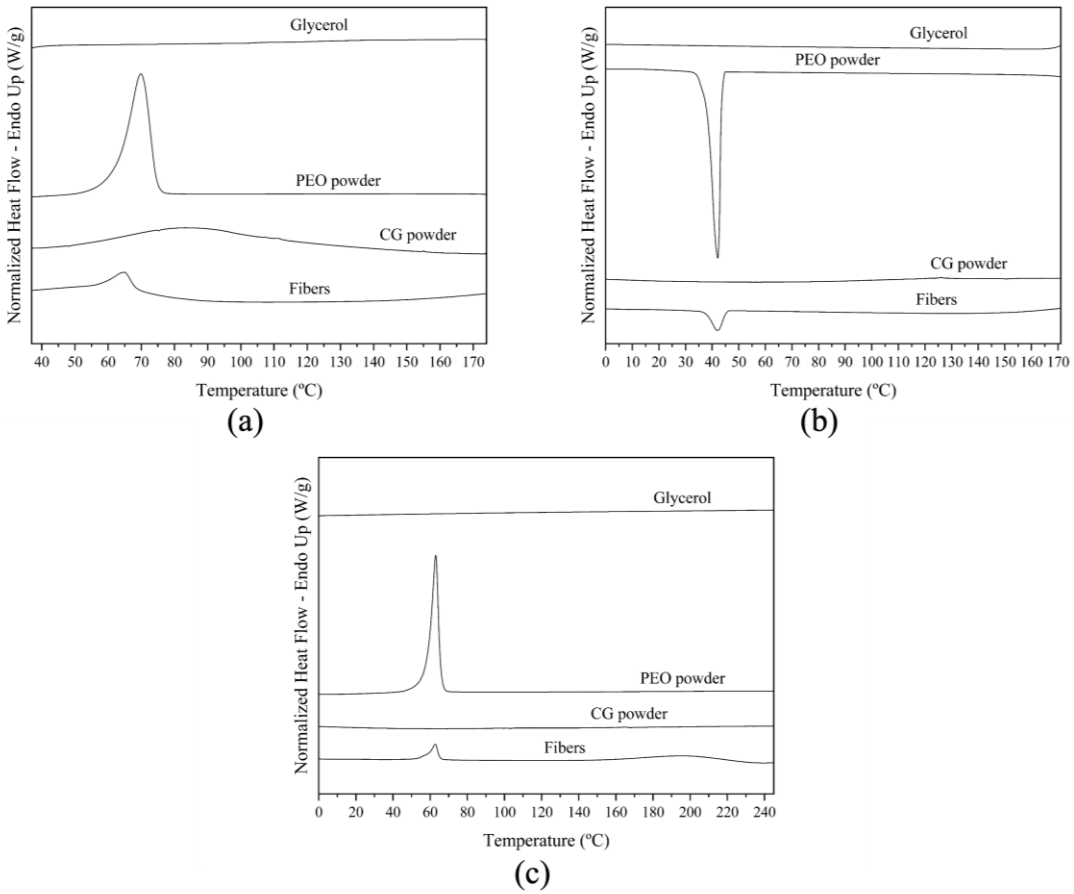

Figure 4. Typical Differential Scanning Calorimetry (DSC) curves of the electrospun fibers from solution *S12* (Fibers), the pure cashew gum (CG), pure PEO_{5M} (PEO), and the pure glycerol. DSC curves are reported during (**a**) first heating step, (**b**) cooling step, and (**c**) second heating step.

The DSC curve of the neat PEO powder during the first thermal step showed an endothermic peak at 71°C with ΔH_m of 202 J/g (Figure 4a), corresponding to its melting event. Similar results were also reported earlier [48] when studying the crystallization kinetics of PEO and its blend with poly(bisphenol A-co-epichlorohydrin). During the second heating run, which was carried out up to higher temperatures (250 °C), a similar endothermic peak but at 61 °C, with ΔH_m of 176 J/g, was reported. Similar results were also reported by Medeiros et al. [49]. During the intermediate cooling step between the thermal runs, the DSC curve of neat PEO powder showed an exothermic peak at 42 °C with ΔH_c of -170 J/g. Kanis et al. reported a crystallization temperature at 53 °C [50]. The DSC curve of neat glycerol did not show any enthalpic features.

The CG:PEO fibers produced with solution *S12* showed clear melting and crystallization peaks associated to the PEO phase. The enthalpies were normalized by the PEO content in the blend, since it was the only crystallizable polymer [51]. During the first heating step the fibers presented one endothermic peak at 65 °C, with ΔH_m of 158 J/g, ascribed to the PEO phase [52]. A reduction of both melting temperature and enthalpy was observed when compared with pure PEO. This could be attributed to an impairment in crystallinity development due to the so called "dilution effect" [53] induced by the presence of CG, but also due to the presence of glycerol [54].

The crystallization temperature and enthalpy of the PEO phase were found at 42 °C and -131 J/g, respectively. During the second heating run the fibers showed an endothermic peak at 63 °C, with ΔH_m of 124 J/g. In this second heating step the peak ascribed to the PEO phase presented a broader endothermic melting peak with a lower temperature shoulder. The observed reduction in enthalpy

 doi:10.20944/preprints202403.0865.v1

compared to the neat PEO was also reported by Cohen and Rocco [48] and they related it to a slower crystallization in the blend, indicating that it was more difficult for PEO crystals to nucleate and grow. A similar behavior of comparative PEO phase enthalpy reduction was also described by Vázquez-González et al. [52] when studying the thermal properties of electrospun fibers based on the FucoPol polysaccharide-PEO blend.

3.3.2. Wide-Angle X-ray Scattering (WAXS)

Wide Angle X-ray Scattering (WAXS) is a technique often used for the investigation of the crystalline phase of materials. It was employed to characterize the crystalline structure of the neat CG, neat PEO_{5M}, and the fibers obtained from solution *S12*. The WAXS diffractograms are presented in Figure 5.

The diffractogram of PEO_{5M} showed numerous peaks due to its semicrystalline nature, with two intense peaks at 24.0, and 19.8°, which were particularly distinctive. Similar results, in the 2θ range of PEO_{5M}, were also found in other studies where, two characteristic diffraction peaks at 23.5° and 19° were clearly visible [55] and were attributed to the (112) and (120) crystallographic planes of PEO_{5M}, respectively [56]. Weak crystalline peaks at 2θ values around 15°, 26°, and 36° were also observed by Lin et al. and Sunderrajan et al. [57,58], confirming the results obtained in this study.

On the contrary, it was not possible to see any distinctive diffraction peak from the diffractogram of CG, confirming its amorphous nature [11] as previously seen by DSC.

The diffractogram of the CG:PEO fibers showed one main peak in the same position as the one found for the neat PEO powder. However, the decrease in relative intensity of this main crystalline peak, which was clearly visible in the diffractogram of the fibers, and the nearly disappearing of the second main peak of PEO_{5M} can be described by a reduction of the crystalline phase [59] as a result of the blending of PEO_{5M} with cashew gum, that influences the organization of the crystallizable component [49] and also for the presence of glycerol, which contributes increasing the amorphous character of the sample [60].

Finally, the neat CG powder exhibited a low angle diffraction peak, which in the blend appeared at an even lower angle, i.e., at around 3°. Diffraction peaks at these low angles have been previously observed and attributed to both helical secondary structures and to other higher hierarchical assemblies [59,61]. The observation here suggests that PEO appears to affect the CG biopolymer hierarchical assembly in a similar fashion as observed before by Vazquez et al. [52] with the FucoPol polysaccharide.

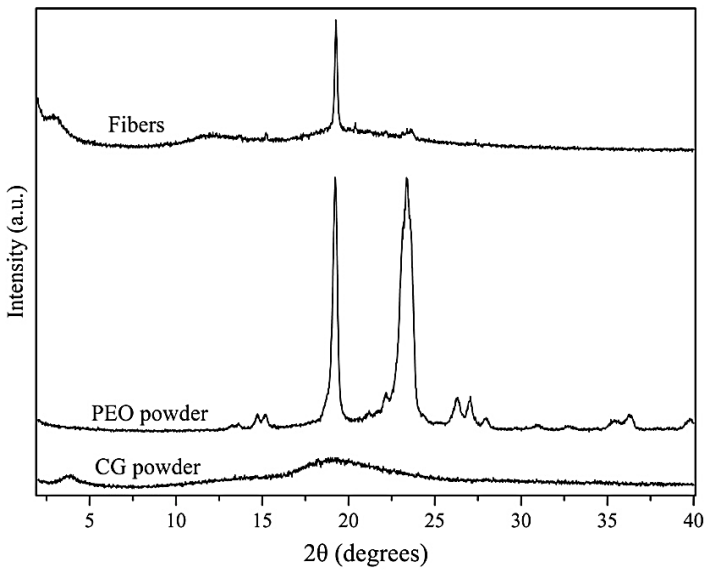

Figure 5. Wide Angle X-ray Scattering (WAXS) patterns of neat cashew gum, neat PEO_{5M} (PEO), and fibers obtained from solution *S12* (Fibers).

 doi:10.20944/preprints202403.0865.v1

3.3.3. Thermogravimetric Analysis

The thermal stability of pure materials and their blends is of paramount importance to screen potential failures during post-processes such as hot filling, humid heat sterilization, and melt compounding [31]. Thermogravimetric analysis (TGA) experiments were carried out for the electrospun fibers from solution *S12*, and for the pure CG and pure PEO_{5M}. The obtained thermograms are gathered in Figure 6.

CG showed two main weight loss steps (Figure 6a). The first step took place between 25 - 125 °C, reporting a weight loss around 10%, which could be attributed to sorbed water evaporation [38]. The second step showed two maximum peaks with degradation temperature (T_{deg}) values of 262 °C and 310 °C, reporting a weight loss of 64% due to the depolymerization of cashew gum [17]. After these two major steps, it was observed a gradual weight loss of around 10% starting from 325 °C. Similar results were obtained by Ferreira et al. [62], who characterized cashew gum and chicha gum for applications in tablets and hydrogels production.

PEO_{5M} showed only one consistent weight loss step of 96%, showing a T_{deg} value of 390 °C (Figure 6b), which was also reported before [52,63]. The neat PEO_{5M} main degradation step relates to the random chain scission of C—O bonds [64,65].

The thermogram of the neat glycerol (Figure 6c) was also determined, in which one main weight loss step of 100% was observed, exhibiting a T_{deg} of 244 °C, which is in accordance with results previously published [66].

From observation of the thermogram of the electrospun fibers (Figure 6d), four clear weight loss steps were seen after an initial 10% weight loss occurred between 25 – 115 °C, which could be attributed to sorbed water evaporation as previously reported for the neat CG. The first main degradation peak was observed at a T_{deg} value of 173 °C and together with the second and the third visible peaks which presented T_{deg} values of 249 °C and 314 °C, respectively, represent a weight loss of around 60%, attributed to the depolymerization of CG [17] and also to the degradation of the glycerol-rich phase [66]. Finally, a fourth weight loss step was observed with maximum at 404 °C, amounting to a weight loss of around 24% as a consequence of the decomposition of PEO_{5M} and to the biopolymer thermal degradation, due to the polysaccharide side chain decomposition [67]. As previously observed [38], the addition of PEO_{5M} and glycerol contributed to reduce the overall thermal stability of the fibers produced since the degradation temperatures occurred at lower values than in the neat components.

 doi:10.20944/preprints202403.0865.v1

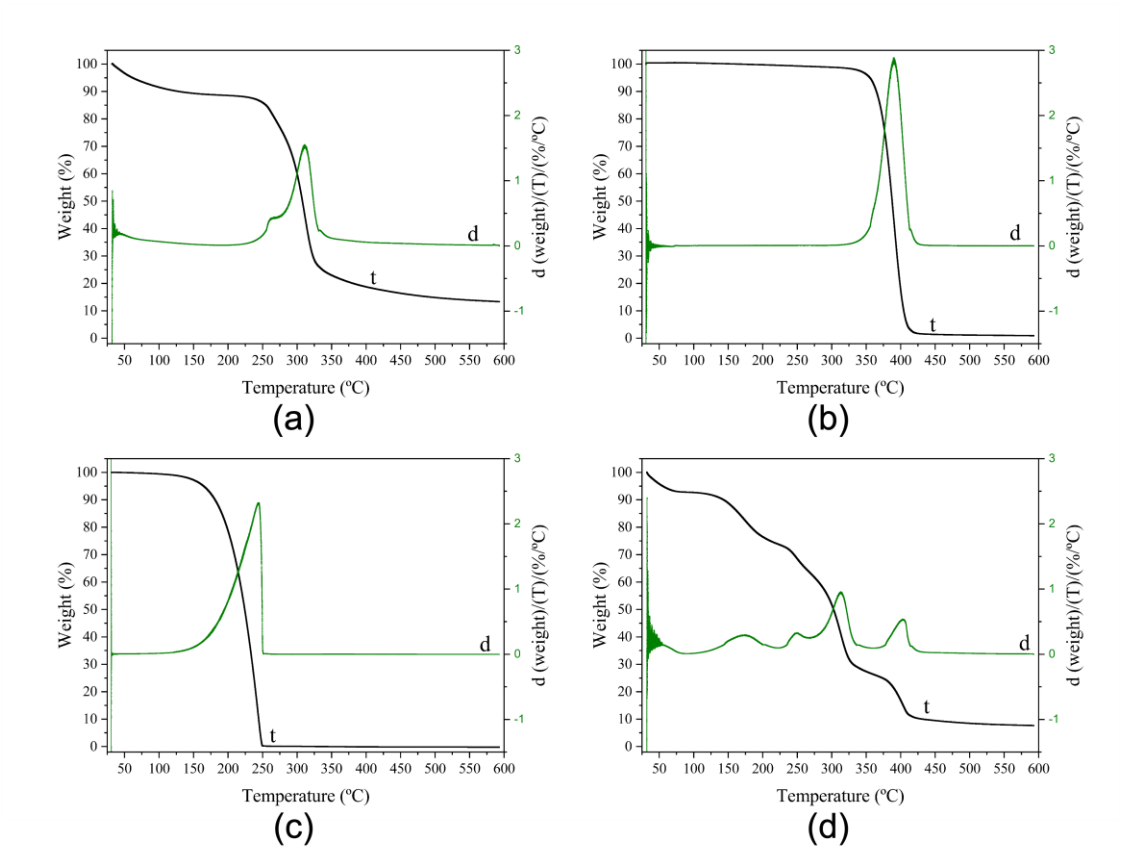

Figure 6. Thermogravimetric analysis (TGA) curves of (**a**) the neat CG, (**b**) the neat PEO_{5M}, (**c**) the neat glycerol, and (**d**) the electrospun fibers from solution *S12*. Where curve t represents the weight loss thermogram, and curve d represents the weight loss first derivative.

3.4. ATR-FTIR Spectroscopy

The ATR-FTIR spectra of the electrospun CG-based fibers from solution *S12*, and of the pure components, that is, the neat PEO_{5M}, neat CG, Span® 20, and glycerol, were taken. The methodology and results can be seen in the Supplementary Materials. No apparent changes were observed comparing the characteristic bands of the ATR-FTIR spectrum of the CG-based fibers to those of the pure components, suggesting the absence of detectable chemical interactions and/or degradation processes.

3.5 Morphology of the Fiber Mats Obtained with Multiple Emitters over a Drum Collector

Figure 7 shows an optical picture of the fiber mat (Figure 7a) and the micrographs of the obtained fibers for sample *S12*, after processing using the high throughput electrospinning setup with a five-needle injector (Figure 7b, 7c, and 7d being micrographs of the same sample taken at different magnifications). The production yield increased from the 3.4 g/h, generated in the single emitter setup, to 38.1 g/h in the high throughput setup. As it can be clearly appreciated in Figures 7a and 7b, the electrospun fibers generated were surprisingly aligned, even though the drum collector speed was very low with respect to yield fiber arrangement per se [68]. More interestingly, the fibers produced here bundled together while flying to the collector in the form of oriented yarns with numerous lateral thinner fiber inter-connections. To the best of our knowledge, this unexpected morphology has never been reported before. This attained morphology occurred spontaneously and was not achieved by means of any fiber deposition control systems, such as additional electrostatic fields different from the one required for the jet initiation [69,70], high drum collector rotation speeds to suppress the whipping motion [68,71,72], jet-deflecting electrodes [73] or electrostatic lens as implemented by Deitzel et al. [74]. The resulting smooth fibers showed a bimodal distribution of sizes

 doi:10.20944/preprints202403.0865.v1

in which bundles of oriented fibers and lateral thinner interconnecting fibers are clearly visible, as already mentioned. The bundled fibers exhibited an average diameter of 45.4 ± 14.9 μm, while the lateral interconnecting fibers presented an average diameter of 4.1 ± 2.2 μm. A bimodal distribution of diameters was also reported before by Urbanek et al. [75] who developed polycaprolactone/chitosan electrospun fibers using a drum collector rotating at 350 rpm, even though no orientation of fibers was observed.

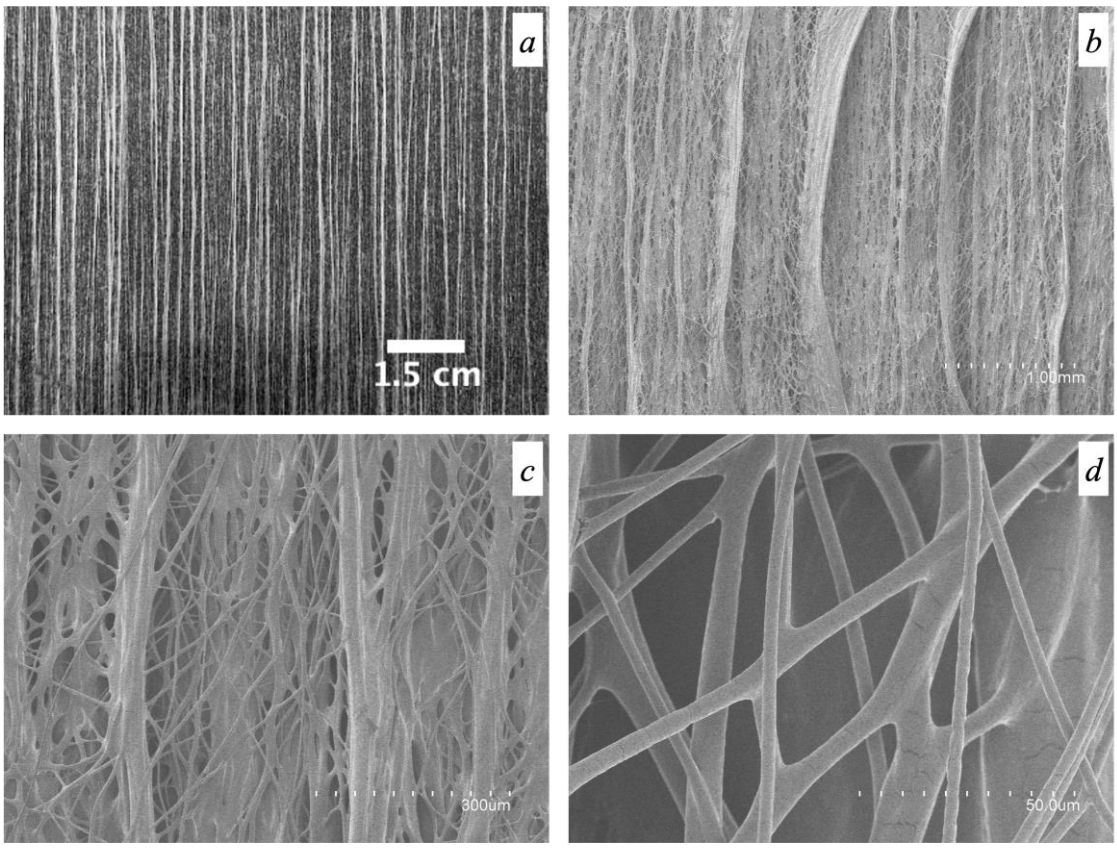

Figure 7. Photograph showing the naked-eye appearance of the electrospun fibers (**a**) and SEM micrographs obtained for solution *S12* using the high throughput electrospinning process (**b**, **c**, and **d**).

In order to better understand the role of both the high-molecular-weight PEO used and glycerol in the attained morphology and mechanical performance of the fiber mat from *S12*, additional experiments were carried out in the same high throughput mode. Thus, fiber mats were produced using the polymeric solutions *Control_1*, *Control_2, and Control_3* (see Table 1). Figure 8 shows the naked eye picture and the SEM micrographs of the electrospun fibers obtained from the polymeric solutions *Control_1*, *Control_2, and Control_3*, which can be directly compared with Figure 7. Fibers from *Control_1*, with an average diameter of 4.8 ± 2.3 μm did show a natural material alignment trend, even though the morphology was completely different from that of the fibers in Figure 7a, i.e., thick bundles of fibers were not generated. Moreover, clearly visible cracks along the mat were seen as a consequence of the extremely high brittleness of the material during handling, which made non-feasible any type of mechanical tensile testing. As already mentioned above, in the single emitter experiments the presence of glycerol as in solution *S12* was considered essential to produce smooth and ductile fibers.

In the case of *Control_2* and *Control_3* fibers, a natural material orientation trend was also observed ascribed to the high molecular weight of the PEO used, even though the morphology was not comparable to that of the blend *S12* (Figure 7). Fibers from *Control_2* and *Control_3* presented an average fiber bundle diameter of 1.3 ± 0.7 μm and 1.3 ± 0.8 μm, respectively. Furthermore, fibers from

 doi:10.20944/preprints202403.0865.v1

Control_3 showed a higher degree of aggregation if compared to those of *Control_2*, which could be due to the presence of the plasticizing and hygroscopic glycerol [76] as binding element for the flying fibers.

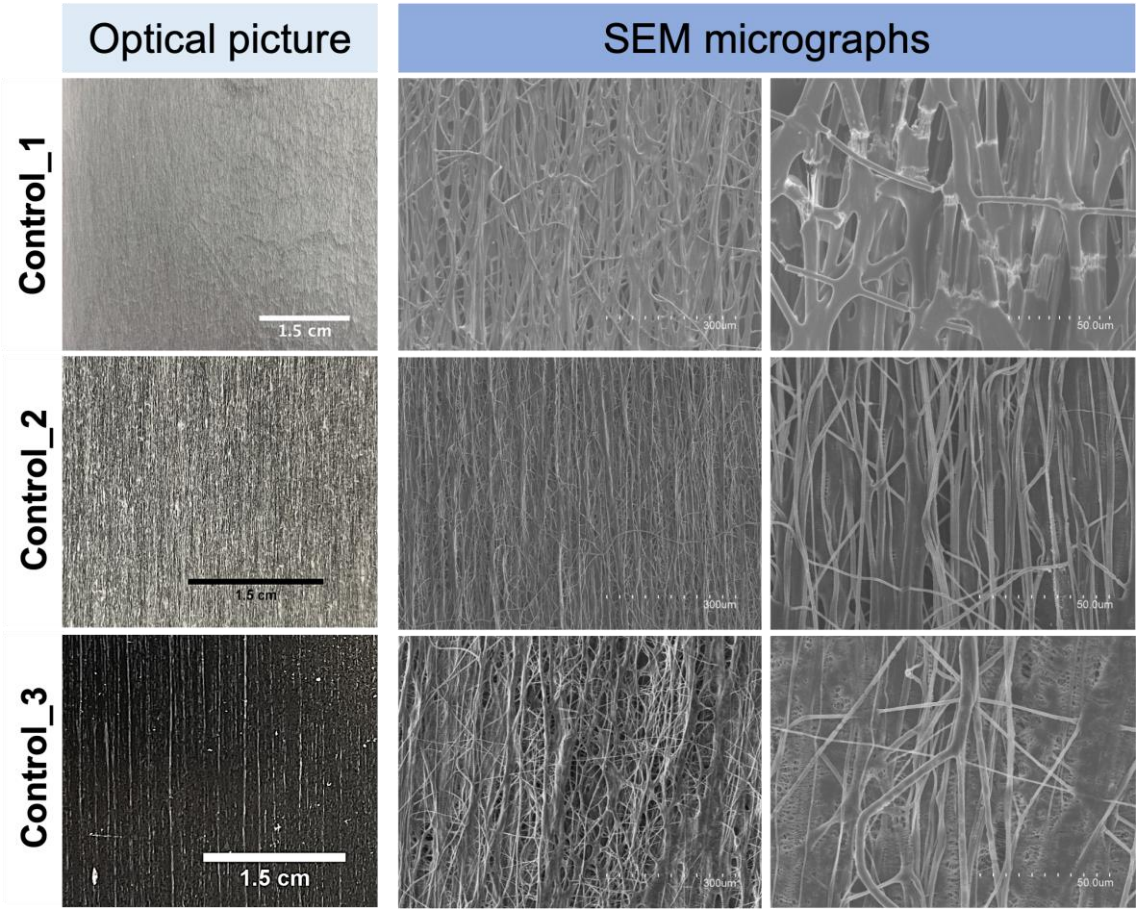

Figure 8. Photographs showing the naked-eye appearance and SEM micrographs of the multi-jet electrospun fiber mats from *Control_1*, *Control_2*, and *Control_3*.

The above experiments (*Control_1* - *Control_3*) suggest that the particular morphology of spontaneous natural fiber alignment into very thick fiber bundles is a unique feature of sample *S12*, contributed by the high content in the mixture of the comb-like branched CG polysaccharide[77,78].

Since spontaneous aligned fibers also occur by processing high-molecular-weight PEO alone, this feature is clearly contributed by the presence of this supporting polymer. This effect on PEO has not been reported before, however spontaneous fiber orientation has been reported before for instance in electrospun fibers based on polystyrene of similar high molecular weight [79]. A contribution to significant fiber bundling seems also to be promoted by glycerol (see *Control_3)*, possibly as a result of the interactions between the CG polysaccharide and the glycerol hydroxyl groups, which bring in efficient electrostatic interactions and hydrogen bonds leading to strong self-association [15,80] during flying towards the collector as the solvent evaporates [81]. Moreover, the presence of glucuronic acid as end-residue in the branched galactan core of CG [13,82–84], imparting a net polyanionic nature to the polysaccharide [13,15], may additionally contribute to the canceling out of the neat charge with the positive charges generated by the high voltage [75], thereby diminishing the overall electric field strength felt by the biopolymer in its flights to the collector, hence helping to suppress the whipping motion and facilitating the strong bundling of the fibers. A similar canceling out charge effect was also reported by Urbanek et al. [75] when processing chitosan/polycaprolactone fibers via electrospinning. They applied a negative polarity at the spinning nozzle that resulted in a reduction of the net positively charged chitosan and thus leading to better

 doi:10.20944/preprints202403.0865.v1

spinnability by reducing the likelihood of jet breaking. However, fiber orientation and bundling were not seen in the latter system.

3.6. Mechanical Properties

Table 4 displays the values of the elastic modulus (*E*), tensile strength at break (σ_b), elongation at break (ε_b), and toughness (T) determined from the strain-stress curve of the high-throughput electrospun samples from *S12*, *Control_1*, *Control_2*, and *Control_3*. The attained *S12* fiber mat presented characteristics of elastomeric materials, showing in the tensile tests high ε_b and T values, above 550 % and 14 mJ/m^3, respectively. As it can be seen, directional alignment of the bundles of fibers allowed a significantly high elongation at break which is a unique morphological feature for *S12* fibers. The presence of the high-molecular-weight PEO is expected to contribute to achieve this superior mechanical elasticity, since *Control_2* and *Control_3* fibers have ε_b values, above 380 % and 340 %, respectively. In a previous study conducted by Vigani et al. [85], it was reported that the addition of small amounts of high molecular weight PEO (4 x 10^6 Da), in alginate-PEO electrospun fibers, resulted in an increase from 1.5 to 10% of the mechanical elongation at break values.

Glycerol is also required to contribute to the observed mechanical properties as can be appreciated from the impossibility to measure the mechanical properties of *Control_1* which has the same formulation of *S12* but without glycerol. The role of glycerol as plasticizer for hydrocolloids is well documented. For instance, Martins et al. [86], reported improved mechanical performance, reaching an elongation at break value of 16 %, by adding 1% w/w of glycerol when producing solution cast CG/chitosan-based films. The role of glycerol as a plasticizing molecule for the mechanical properties of hydrophilic polymers originates by the synergetic contributions of two main phenomena, namely the reduction of the intermolecular forces between polymer chains and the subsequent promotion of chain mobility [87], and its ability to sorb moisture [88,89]. In our work, a small quantity of glycerol was able to contribute to generate a tremendously high elongation at break for the specific electrospun fiber mats developed. Indeed, higher quantities of glycerol have been usually required to achieve significant elasticity enhancements, as reported earlier in the literature. For instance, Farshi et al. [90] reached an elongation at break value of 106% by adding a 12% w/w of glycerol in silk fibroin/carboxymethyl cellulose-based films. In another recent work carried out by Nagakawa et al. [91], an elongation at break value of 93% was attained by adding a 15% w/w of glycerol in poly (vinyl alcohol) nanofibrous cryogels.

The fiber mat from *S12* showed reduced mechanical properties when the analysis was performed perpendicular to the rolling direction, as seen from Table 4. This is in agreement with the morphological results seen in Figure 7, pointing to a weaker inter-fiber cohesion along the sample width.

Table 4. Mechanical properties in terms of tensile modulus (E), tensile strength at break (σ_b), elongation at break (ε_b), and toughness (T) of the electrospun fibers obtained from S12 and Control_1, Control_2, and Control_3 in the drum rolling direction (RD) and transversal direction (TD).

Sample	*Measurement Direction*	*E* (MPa)	σ_b (MPa)	ε_b (%)	T (mJ/m^3)
Fibers from *S12*	RD	78 ± 23^a	3.7 ± 1.4^c	550 ± 54^a	14 ± 5^b
	TD	67 ± 39^a	0.6 ± 0.1^c	225 ± 17^b	1 ± 0^c
Control_1	RD	n.a.	n.a.	n.a.	n.a.
	TD	n.a.	n.a.	n.a.	n.a.
Control_2	RD	64 ± 3^a	26 ± 2^b	380 ± 46^b	69 ± 12^a
	TD	13 ± 1^a	3.6 ± 0.2^b	147 ± 18^b	3.8 ± 0.6^b
Control_3	RD	54 ± 4^a	79 ± 5^a	341 ± 7^b	64 ± 9^a
	TD	24 ± 3^a	20 ± 2^a	332 ± 56^a	47 ± 7^a

 doi:10.20944/preprints202403.0865.v1

*Each column represents the mean value ± standard deviation of three independent replicas. Different letters in the same column indicate a significant difference among the samples ($p < 0.05$). Statistical analysis was performed comparing samples of the same measurement direction (e.g. RD or TD).

4. Conclusions

To the best of our knowledge, this is the first research study dealing with the production of highly stretchable CG-based materials by electrospinning. From the results, it was not possible to obtain pure CG electrospun fibers; however, electrospun fibers were successfully produced by blending CG with a high molecular weight polyethylene oxide supporting polymer. The resultant electrospun fibers presented a smooth and continuous structure. However, the presence of beads or spindle-like defects were also detected in the electrospun fibers. The removal of the impurities from solubilized CG by means of centrifugation, together with the use of a 3.5% w/w of pure glycerol as plasticizer, allowed the successful generation of fibers free of both beads and spindle-like defects, as determined by scanning electron microscopy (SEM). Thermal transitions and thermal stability of the samples were assessed by differential scanning calorimetry (DSC) and thermogravimetric analysis (TGA), respectively, confirming a reduction of CG thermal stability by the addition of PEO, and a reduction of PEO crystallinity as a result of blending the polymer with CG.

In addition, when the selected formula was electrospun over a drum collector, rotating at a very low rotational speed, from multiple emitters, very thick aligned fiber bundles, never reported before, were obtained in the rotational direction with thinner interconnecting fibers between the bundles in the transverse direction. Such natural fiber orientation was hypothesized to be the synergic result of both the presence of small quantities of a high-molecular weight supporting polymer, that is PEO_{5M}, and glycerol. The obtained fiber mat presented a very impressive elastic behavior in the direction of the aligned fibers, exhibiting a tensile modulus (E) of 78 MPa and an elongation at break value (ε_b) of 550 %. These properties potentially make this material, obtained by blending CG with PEO_{5M}, a potential sustainable alternative to conventional elastomers.

Furthermore, the promising results achieved in this work together with the low cost and the high availability in nature of cashew gum, as raw material, along with other positive properties such as its biocompatibility and safety, make this bio-based polysaccharide a material of interest for future investigations in several fields requiring non-direct aqueous contact biobased materials with elastic properties. Further research in this area holds promise for advancing materials science and technology.

5. Patents

Part of the results of this study were filed in a Spanish patent application, ES16411784.

Supplementary Materials: The following supporting information can be downloaded at the website of this paper posted on Preprints.org.

Author Contributions: Conceptualization J.M.L.; methodology, validation, and formal analysis M.G., C.P., L.C.; investigation, resources, data curation, writing-original draft preparation, review and editing M.G., C.P., S.L., H.N.C., A.B., R.F.F. and J.M.L.; visualization, supervision, project administration and funding acquisition J.M.L. All authors have read and agreed to the published version of the manuscript.

Funding: This study was supported by the Agencia Valenciana de Innovación (AVI), project INNEST/2022/25 and by the Spanish Ministry of Science Innovation and Universities (MCIU), project PID2021-128749OB-C31.

Institutional Review Board Statement: Mention of trade names or commercial products in this publication is solely for the purpose of providing specific information and does not imply recommendation or endorsement by the U.S. Department of Agriculture. USDA is an equal opportunity provider and employer.

Acknowledgments: Mattia Grumi acknowledges the scholarship "Call for Thesis Abroad 2019/2020 for deserving students" awarded by Università degli Studi di Milano. The authors would also like to acknowledge the Unidad Asociada IATA(CSIC)-UJI in "Polymer Technology" and the CSIC-PTI SusPlast and Maria Pardo from IATA-CSIC for technical support during the execution of the multi-jet experiments. The Accreditation as Center of Excellence Severo Ochoa CEX2021-001189-S funded by MCIU/AEI/10.13039/501100011033 is also fully acknowledged.

Conflicts of Interest: The authors declare no conflicts of interest.

References

1. Andrade, M.S.; Ishikawa, O.H.; Costa, R.S.; Seixas, M.V.S.; Rodrigues, R.C.L.B.; Moura, E.A.B. Development of Sustainable Food Packaging Material Based on Biodegradable Polymer Reinforced with Cellulose Nanocrystals. Food Packag Shelf Life 2022, 31, 100807, doi:https://doi.org/10.1016/j.fpsl.2021.100807.
2. Chausali, N.; Saxena, J.; Prasad, R. Recent Trends in Nanotechnology Applications of Bio-Based Packaging. *J Agric Food Res* **2022**, *7*, 100257, doi:https://doi.org/10.1016/j.jafr.2021.100257.
3. Piscopo, A.; Zappia, A.; de Bruno, A.; Pozzo, S.; Limbo, S.; Piergiovanni, L.; Poiana, M. Use of Biodegradable Materials as Alternative Packaging of Typical Calabrian Provola Cheese. *Food Packag Shelf Life* **2019**, *21*, 100351, doi:https://doi.org/10.1016/j.fpsl.2019.100351.
4. Amaral, R.G.; de Andrade, L.R.M.; Andrade, L.N.; Loureiro, K.C.; Souto, E.B.; Severino, P. Cashew Gum: A Review of Brazilian Patents and Pharmaceutical Applications with a Special Focus on Nanoparticles. *Micromachines (Basel)* **2022**, *13*, 1137, doi:10.3390/mi13071137.
5. Prajapati, V.D.; Jani, G.K.; Moradiya, N.G.; Randeria, N.P. Pharmaceutical Applications of Various Natural Gums, Mucilages and Their Modified Forms. *Carbohydr Polym* **2013**, *92*, 1685–1699, doi:10.1016/j.carbpol.2012.11.021.
6. Munir, H.; Bilal, M.; Khan, M.I.; Iqbal, H.M.N. Gums-Based Bionanostructures for Medical Applications. In *Polysaccharides*; Wiley Online Books; Wiley, 2021; pp. 385–398.
7. Ribeiro, A.J.; de Souza, F.R.L.; Bezerra, J.M.N.A.; Oliveira, C.; Nadvorny, D.; de La Roca Soares, M.F.; Nunes, L.C.C.; Silva-Filho, E.C.; Veiga, F.; Soares Sobrinho, J.L. Gums' Based Delivery Systems: Review on Cashew Gum and Its Derivatives. *Carbohydr Polym* **2016**, *147*, 188–200, doi:10.1016/j.carbpol.2016.02.042.
8. Carvalho da Silva, L.; Alves do Nascimento, M.; Guabiraba Mendes, L.; Ferro Furtado, R.; Correia da Costa, J.M.; Luiz Herzog Cardoso, A. Optimization of Cashew Gum and Chitosan for Microencapsulation of Pequi Oil by Complex Coacervation. *J Food Process Preserv* **2018**, *42*, e13538, doi:10.1111/jfpp.13538.
9. Cheng, H.N.; Furtado, R.F.; Biswas, A.; Alves, C.; Prieto, C.; Lagaron, J.M. Chemical Modifications and Applications of Cashew Byproducts - A Selective Review. *ACS Food Science & Technology* **2022**, doi:10.1021/acsfoodscitech.2c00168.
10. Silva, S.M.F.; Ribeiro, H.L.; Mattos, A.L.A.; Borges, M. de F.; Rosa, M. de F.; de Azeredo, H.M.C. Films from Cashew Byproducts: Cashew Gum and Bacterial Cellulose from Cashew Apple Juice. *J Food Sci Technol* **2021**, *58*, 1979–1986, doi:10.1007/s13197-020-04709-7.
11. Andrade, K.C.S.; Carvalho, C.W.P. de; Takeiti, C.Y.; Azeredo, H.M.C. de; Corrêa, J. da S.; Caldas, C.M. Goma de Cajueiro (Anacardium Occidentale): Avaliação Das Modificações Químicas e Físicas Por Extrusão Termoplástica. *Polímeros Ciência e Tecnologia* **2013**, *23*, 667–671, doi:10.4322/polimeros.2013.004.
12. de Paula, R.C.M.; Rodrigues, J.F. Composition and Rheological Properties of Cashew Tree Gum, the Exudate Polysaccharide from Anacardium Occidentale L. *Carbohydr Polym* **1995**, *26*, 177–181, doi:10.1016/0144-8617(95)00006-S.
13. Kumar, A.; Moin, A.; R, S.; Ahmed, A.; G. Shivakumar, H. Cashew Gum A Versatile Hydrophyllic Polymer: A Review. *Curr Drug ther* **2012**, *7*, 2–12, doi:10.2174/157488512800389146.
14. Silva, F.E.F.; Batista, K.A.; Di-Medeiros, M.C.B.; Silva, C.N.S.; Moreira, B.R.; Fernandes, K.F. A Stimuli-Responsive and Bioactive Film Based on Blended Polyvinyl Alcohol and Cashew Gum Polysaccharide. *Materials Science and Engineering C* **2016**, *58*, 927–934, doi:10.1016/j.msec.2015.09.064.
15. Azevedo, G.A.; Heinrichs, M.C.; Moraes, Â.M. Cashew Tree Gum for Biomaterials Engineering: A Versatile Raw Material in Consolidation. *J Appl Polym Sci* **2022**, *139*, doi:10.1002/app.52484.
16. Gyedu-Akoto, E.; Amoah, F.M.; Oduro, I. Cashew Tree (Anarcadium Occidentale L.) Exudate Gum. *Emerging Natural Hydrocolloids: Rheology and Functions* **2019**, 327–346, doi:10.1002/9781119418511.ch13.
17. Vázquez-González, Y.; Prieto, C.; Filizoglu, M.F.; Ragazzo-Sánchez, J.A.; Calderón-Santoyo, M.; Furtado, R.F.; Cheng, H.N.; Biswas, A.; Lagaron, J.M. Electrosprayed Cashew Gum Microparticles for the Encapsulation of Highly Sensitive Bioactive Materials. *Carbohydr Polym* **2021**, *264*, doi:10.1016/j.carbpol.2021.118060.
18. Porto, B.C.; Augusto, P.E.D.; Cristianini, M. A Comparative Study Between Technological Properties of Cashew Tree Gum and Arabic Gum. *J Polym Environ* **2015**, *23*, 392–399, doi:10.1007/s10924-014-0698-z.
19. Sameen, D.E.; Ahmed, S.; Lu, R.; Li, R.; Dai, J.; Qin, W.; Zhang, Q.; Li, S.; Liu, Y. Electrospun Nanofibers Food Packaging: Trends and Applications in Food Systems. *Crit Rev Food Sci Nutr* **2021**, *0*, 1–14, doi:10.1080/10408398.2021.1899128.
20. Subbiah, T.; Bhat, G.S.; Tock, R.W.; Parameswaran, S.; Ramkumar, S.S. Electrospinning of Nanofibers. *J Appl Polym Sci* **2005**, *96*, 557–569, doi:10.1002/app.21481.

21. Torres-Giner, S.; Busolo, M.; Cherpinski, A.; Lagaron, J.M. CHAPTER 10 Electrospinning in the Packaging Industry. In *Electrospinning: From Basic Research to Commercialization*; The Royal Society of Chemistry, 2018; pp. 238–260 ISBN 978-1-78801-100-6.
22. Doshi, J.; Reneker, D.H. Electrospinning Process and Applications of Electrospun Fibers. *J Electrostat* **1995**, *35*, 151–160, doi:10.1016/0304-3886(95)00041-8.
23. Greiner, A.; Wendorff, J.H. Electrospinning: A Fascinating Method for the Preparation of Ultrathin Fibers. *Angewandte Chemie International Edition* **2007**, *46*, 5670–5703, doi:10.1002/anie.200604646.
24. Haider, A.; Haider, S.; Kang, I.-K. A Comprehensive Review Summarizing the Effect of Electrospinning Parameters and Potential Applications of Nanofibers in Biomedical and Biotechnology. *Arabian Journal of Chemistry* **2018**, *11*, 1165–1188, doi:10.1016/j.arabjc.2015.11.015.
25. Yan, X.; Yao, H.; Luo, J.; Li, Z.; Wei, J. Functionalization of Electrospun Nanofiber for Bone Tissue Engineering. *Polymers (Basel)* **2022**, *14*, doi:10.3390/polym14142940.
26. Teno, J.; Pardo-Figuerez, M.; Figueroa-Lopez, K.J.; Prieto, C.; Lagaron, J.M. Development of Multilayer Ciprofloxacin Hydrochloride Electrospun Patches for Buccal Drug Delivery. *J Funct Biomater* **2022**, *13*, 170, doi:10.3390/jfb13040170.
27. Prieto, C.; Talón, E.; Noreña, C.Z.; Lagaron, J.M. Effect of Whey Protein Purity on the Characteristics of Algae Oil-Loaded Encapsulates Obtained by Electrospraying Assisted by Pressurized Gas. *Nanomaterials* **2022**, *12*, 3096, doi:10.3390/nano12183096.
28. Hernaez, B.; Muñoz-Gómez, A.; Sanchiz, A.; Orviz, E.; Valls-Carbo, A.; Sagastagoitia, I.; Ayerdi, O.; Martín, R.; Puerta, T.; Vera, M.; et al. Monitoring Monkeypox Virus in Saliva and Air Samples in Spain: A Cross-Sectional Study. *Lancet Microbe* **2023**, *4*, e21–e28, doi:10.1016/S2666-5247(22)00291-9.
29. Lagarón, J.-M. Multifunctional and Nanoreinforced Polymers for Food Packaging. In *Multifunctional and Nanoreinforced Polymers for Food Packaging*; Lagarón, J.-M.B.T.-M. and N.P. for F.P., Ed.; Elsevier, 2011; pp. 1–28.
30. Figueroa-Lopez, K.J.; Cabedo, L.; Lagaron, J.M.; Torres-Giner, S. Development of Electrospun Poly(3-Hydroxybutyrate-Co-3-Hydroxyvalerate) Monolayers Containing Eugenol and Their Application in Multilayer Antimicrobial Food Packaging. *Front Nutr* **2020**, *7*, doi:10.3389/fnut.2020.00140.
31. Figueroa-Lopez, K.; Castro-Mayorga, J.; Andrade-Mahecha, M.; Cabedo, L.; Lagaron, J. Antibacterial and Barrier Properties of Gelatin Coated by Electrospun Polycaprolactone Ultrathin Fibers Containing Black Pepper Oleoresin of Interest in Active Food Biopackaging Applications. *Nanomaterials* **2018**, *8*, 199, doi:10.3390/nano8040199.
32. Figueroa-Lopez, K.J.; Torres-Giner, S.; Enescu, D.; Cabedo, L.; Cerqueira, M.A.; Pastrana, L.M.; Lagaron, J.M. Electrospun Active Biopapers of Food Waste Derived Poly(3-Hydroxybutyrate-Co-3-Hydroxyvalerate) with Short-Term and Long-Term Antimicrobial Performance. *Nanomaterials* **2020**, *10*, 506, doi:10.3390/nano10030506.
33. Melendez-Rodriguez, B.; Reis, M.A.M.; Carvalheira, M.; Sammon, C.; Cabedo, L.; Torres-Giner, S.; Lagaron, J.M. Development and Characterization of Electrospun Biopapers of Poly(3-Hydroxybutyrate- *Co* -3-Hydroxyvalerate) Derived from Cheese Whey with Varying 3-Hydroxyvalerate Contents. *Biomacromolecules* **2021**, *22*, 2935–2953, doi:10.1021/acs.biomac.1c00353.
34. Melendez-Rodriguez, B.; Castro-Mayorga, J.L.; Reis, M.A.M.; Sammon, C.; Cabedo, L.; Torres-Giner, S.; Lagaron, J.M. Preparation and Characterization of Electrospun Food Biopackaging Films of Poly(3-Hydroxybutyrate-Co-3-Hydroxyvalerate) Derived From Fruit Pulp Biowaste. *Front Sustain Food Syst* **2018**, *2*, 1–16, doi:10.3389/fsufs.2018.00038.
35. Oliveira, M.A.; Furtado, R.F.; Bastos, M.S.R.; Leitão, R.C.; Benevides, S.D.; Muniz, C.R.; Cheng, H.N.; Biswas, A. Performance Evaluation of Cashew Gum and Gelatin Blend for Food Packaging. *Food Packag Shelf Life* **2018**, *17*, 57–64, doi:10.1016/j.fpsl.2018.05.003.
36. de Souza, W.F.C.; de Lucena, F.A.; da Silva, K.G.; Martins, L.P.; de Castro, R.J.S.; Sato, H.H. Influence of Edible Coatings Composed of Alginate, Galactomannans, Cashew Gum, and Gelatin on the Shelf- Life of Grape Cultivar 'Italia': Physicochemical and Bioactive Properties. *LWT* **2021**, *152*, 112315, doi:https://doi.org/10.1016/j.lwt.2021.112315.
37. da Silva, D.P.B.; Florentino, I.F.; da Silva Moreira, L.K.; Brito, A.F.; Carvalho, V.V.; Rodrigues, M.F.; Vasconcelos, G.A.; Vaz, B.G.; Pereira-Junior, M.A.; Fernandes, K.F.; et al. Chemical Characterization and Pharmacological Assessment of Polysaccharide Free, Standardized Cashew Gum Extract (Anacardium Occidentale L.). *J Ethnopharmacol* **2018**, *213*, 395–402, doi:10.1016/j.jep.2017.11.021.
38. Akinalan Balik, B.; Argin, S.; Lagaron, J.M.; Torres-Giner, S. Preparation and Characterization of Electrospun Pectin-Based Films and Their Application in Sustainable Aroma Barrier Multilayer Packaging. *Applied Sciences* **2019**, *9*, 5136, doi:10.3390/app9235136.

39. Liang, Q.; Pan, W.; Gao, Q. Preparation of Carboxymethyl Starch/Polyvinyl-Alcohol Electrospun Composite Nanofibers from a Green Approach. *Int J Biol Macromol* **2021**, *190*, 601–606, doi:10.1016/j.ijbiomac.2021.09.015.
40. Ramos-Hernández, J.; Ragazzo-Sánchez, J.; Calderón-Santoyo, M.; Ortiz-Basurto, R.; Prieto, C.; Lagaron, J. Use of Electrosprayed Agave Fructans as Nanoencapsulating Hydrocolloids for Bioactives. *Nanomaterials* **2018**, *8*, 868, doi:10.3390/nano8110868.
41. Gómez-Mascaraque, L.G.; Perez-Masiá, R.; González-Barrio, R.; Periago, M.J.; López-Rubio, A. Potential of Microencapsulation through Emulsion-Electrospraying to Improve the Bioaccesibility of β-Carotene. *Food Hydrocoll* **2017**, *73*, 1–12, doi:10.1016/j.foodhyd.2017.06.019.
42. Librán, C.M.; Castro, S.; Lagaron, J.M. Encapsulation by Electrospray Coating Atomization of Probiotic Strains. *Innovative Food Science & Emerging Technologies* **2017**, *39*, 216–222, doi:10.1016/j.ifset.2016.12.013.
43. Fong, H.; Chun, I.; Reneker, D.H. Beaded Nanofibers Formed during Electrospinning. *Polymer (Guildf)* **1999**, *40*, 4585–4592, doi:10.1016/S0032-3861(99)00068-3.
44. Yu, J.; Qiu, Y.; Zha, X.; Yu, M.; Yu, J.; Rafique, J.; Yin, J. Production of Aligned Helical Polymer Nanofibers by Electrospinning. *Eur Polym J* **2008**, *44*, 2838–2844, doi:10.1016/j.eurpolymj.2008.05.020.
45. Gibis, M.; Pribek, F.; Kutzli, I.; Weiss, J. Influence of the Protein Content on Fiber Morphology and Heat Treatment of Electrospun Potato Protein–Maltodextrin Fibers. *Applied Sciences* **2021**, *11*, 7896, doi:10.3390/app11177896.
46. Cui, S.-S.; Sun, X.; Yao, B.; Peng, X.-X.; Zhang, X.-T.; Zhou, Y.-F.; Hu, J.-L.; Liu, Y.-C. Size-Tunable Low Molecular Weight Pectin-Based Electrospun Nanofibers Blended with Low Content of Poly(Ethylene Oxide). *J Nanosci Nanotechnol* **2017**, *17*, 681–689, doi:10.1166/jnn.2017.12540.
47. Guerreiro, B.M.; Freitas, F.; Lima, J.C.; Silva, J.C.; Dionísio, M.; Reis, M.A.M. Demonstration of the Cryoprotective Properties of the Fucose-Containing Polysaccharide FucoPol. *Carbohydr Polym* **2020**, *245*, 116500, doi:https://doi.org/10.1016/j.carbpol.2020.116500.
48. Cohen, L.E.; Rocco, A.M. Study of the Crystallization Kinetics Poly(Ethylene Oxide) and a Blend of Poly(Ethylene Oxide) and Poly(Bisphenol A-Co-Epichlorohydrin). *J Therm Anal Calorim* **2000**, *59*, 625–632, doi:10.1023/A:1010168729446.
49. Medeiros, G.B.; Souza, P.R.; Retamiro, K.M.; Nakamura, C.V.; Muniz, E.C.; Corradini, E. Experimental Design to Evaluate Properties of Electrospun Fibers of Zein/Poly (Ethylene Oxide) for Biomaterial Applications. *J Appl Polym Sci* **2021**, *138*, 50898, doi:10.1002/app.50898.
50. Kanis, L.A.; Viel, F.C.; Crespo, J.S.; Bertolino, J.R.; Pires, A.T.N.; Soldi, V. Study of Poly(Ethylene Oxide)/Carbopol Blends through Thermal Analysis and Infrared Spectroscopy. *Polymer (Guildf)* **2000**, *41*, 3303–3309, doi:10.1016/S0032-3861(99)00520-0.
51. Lu, C.; Chiang, S.W.; Du, H.; Li, J.; Gan, L.; Zhang, X.; Chu, X.; Yao, Y.; Li, B.; Kang, F. Thermal Conductivity of Electrospinning Chain-Aligned Polyethylene Oxide (PEO). *Polymer (Guildf)* **2017**, *115*, 52–59, doi:10.1016/j.polymer.2017.02.024.
52. Vázquez-González, Y.; Prieto, C.; Stojanovic, M.; Torres, C.A.V.; Freitas, F.; Ragazzo-Sánchez, J.A.; Calderón-Santoyo, M.; Lagaron, J.M. Preparation and Characterization of Electrospun Polysaccharide FucoPol-Based Nanofiber Systems. *Nanomaterials* **2022**, *12*, doi:10.3390/nano12030498.
53. Arai, F.; Shinohara, K.; Nagasawa, N.; Takeshita, H.; Takenaka, K.; Miya, M.; Shiomi, T. Crystallization Behavior and Higher-Order Structure in Miscible Crystalline/Crystalline Polymer Blends. *Polym J* **2013**, *45*, 921–928, doi:10.1038/pj.2013.5.
54. Hubackova, J.; Dvorackova, M.; Svoboda, P.; Mokrejs, P.; Kupec, J.; Pozarova, I.; Alexy, P.; Bugaj, P.; Machovsky, M.; Koutny, M. Influence of Various Starch Types on PCL/Starch Blends Anaerobic Biodegradation. *Polym Test* **2013**, *32*, 1011–1019, doi:10.1016/j.polymertesting.2013.05.008.
55. Abdollahi, S.; Ehsani, M.; Morshedian, J.; Khonakdar, H.A.; Reuter, U. Structural and Electrochemical Properties of PEO/PAN Nanofibrous Blends: Prediction of Graphene Localization. *Polym Compos* **2018**, *39*, 3626–3635, doi:10.1002/pc.24390.
56. Zhang, L.; Hsieh, Y. lo Nanoporous Ultrahigh Specific Surface Polyacrylonitrile Fibres. *Nanotechnology* **2006**, *17*, 4416–4423, doi:10.1088/0957-4484/17/17/022.
57. Lin, H.; Kai, T.; Freeman, B.D.; Kalakkunnath, S.; Kalika, D.S. The Effect of Cross-Linking on Gas Permeability in Cross-Linked Poly(Ethylene Glycol Diacrylate). *Macromolecules* **2005**, *38*, 8381–8393, doi:10.1021/ma0510136.
58. Sunderrajan, S.; Freeman, B.D.; Hall, C.K.; Pinnau, I. Propane and Propylene Sorption in Solid Polymer Electrolytes Based on Poly(Ethylene Oxide) and Silver Salts. *J Memb Sci* **2001**, *182*, 1–12, doi:10.1016/S0376-7388(00)00569-X.

59. Khan, M.A.; Zhou, C.; Zheng, P.; Zhao, M.; Liang, L. Improving Physicochemical Stability of Quercetin-Loaded Hollow Zein Particles with Chitosan/Pectin Complex Coating. *Antioxidants* **2021**, *10*, 1476, doi:10.3390/antiox10091476.
60. Pasini Cabello, S.D.; Takara, E.A.; Marchese, J.; Ochoa, N.A. Influence of Plasticizers in Pectin Films: Microstructural Changes. *Mater Chem Phys* **2015**, *162*, 491–497, doi:https://doi.org/10.1016/j.matchemphys.2015.06.019.
61. Diener, M. Structural Hierarchy in Linear Polysaccharides-from the Nano-to Macroscale. Ph.D. Thesis, ETH Zurich: Zurich, 2020.
62. Ferreira, S.R. dos S.; Mesquita, M.V.N.; Sá, L.L.F. de; Nogueira, N.C.; Rizzo, M. dos S.; Silva-Filho, E.C.; Costa, M.P. da; Ribeiro, A.B. Sustainable Natural Gums for Industrial Application: Physiochemical and Texturometric Evaluation. *J Drug Deliv Sci Technol* **2019**, *54*, 101306, doi:10.1016/j.jddst.2019.101306.
63. Bozkaya, O.; Arat, E.; Gün Gök, Z.; Yiğitoğlu, M.; Vargel, İ. Production and Characterization of Hybrid Nanofiber Wound Dressing Containing Centella Asiatica Coated Silver Nanoparticles by Mutual Electrospinning Method. *Eur Polym J* **2022**, *166*, 111023, doi:https://doi.org/10.1016/j.eurpolymj.2022.111023.
64. Costa, C.M.; MacHiavello, M.N.T.; Ribelles, J.L.G.; Lanceros-Méndez, S. Composition-Dependent Physical Properties of Poly[(Vinylidene Fluoride)-Co-Trifluoroethylene]-Poly(Ethylene Oxide) Blends. *J Mater Sci* **2013**, *48*, 3494–3504, doi:10.1007/s10853-013-7141-z.
65. Jakić, M.; Stipanelov Vrandečić, N.; Erceg, M. Thermal Degradation of Poly(3-Hydroxybutyrate)/Poly(Ethylene Oxide) Blends: Thermogravimetric and Kinetic Analysis. *Eur Polym J* **2016**, *81*, 376–385, doi:https://doi.org/10.1016/j.eurpolymj.2016.06.024.
66. García, N.L.; Famá, L.; Dufresne, A.; Aranguren, M.; Goyanes, S. A Comparison between the Physico-Chemical Properties of Tuber and Cereal Starches. *Food Research International* **2009**, *42*, 976–982, doi:10.1016/j.foodres.2009.05.004.
67. Vendruscolo, C.W.; Ferrero, C.; Pineda, E.A.G.; Silveira, J.L.M.; Freitas, R.A.; Jiménez-Castellanos, M.R.; Bresolin, T.M.B. Physicochemical and Mechanical Characterization of Galactomannan from Mimosa Scabrella: Effect of Drying Method. *Carbohydr Polym* **2009**, *76*, 86–93, doi:https://doi.org/10.1016/j.carbpol.2008.09.028.
68. Tong, H.-W.; Wang, M. Electrospinning of Aligned Biodegradable Polymer Fibers and Composite Fibers for Tissue Engineering Applications. *J Nanosci Nanotechnol* **2007**, *7*, 3834–3840, doi:10.1166/jnn.2007.051.
69. Li, D.; Wang, Y.; Xia, Y. Electrospinning of Polymeric and Ceramic Nanofibers as Uniaxially Aligned Arrays. *Nano Lett* **2003**, *3*, 1167–1171, doi:10.1021/nl0344256.
70. Bellan, L.M.; Craighead, H.G. Applications of Controlled Electrospinning Systems. *Polym Adv Technol* 2011, *22*, 304–309.
71. Alfaro De Prá, M.A.; Ribeiro-do-Valle, R.M.; Maraschin, M.; Veleirinho, B. Effect of Collector Design on the Morphological Properties of Polycaprolactone Electrospun Fibers. *Mater Lett* **2017**, *193*, 154–157, doi:10.1016/j.matlet.2017.01.102.
72. Kiselev, P.; Rosell-Llompart, J. Highly Aligned Electrospun Nanofibers by Elimination of the Whipping Motion. *J Appl Polym Sci* **2012**, *125*, 2433–2441, doi:10.1002/app.36519.
73. Liashenko, I.; Rosell-Llompart, J.; Cabot, A. Ultrafast 3D Printing with Submicrometer Features Using Electrostatic Jet Deflection. *Nat Commun* **2020**, *11*, 753, doi:10.1038/s41467-020-14557-w.
74. Deitzel, J. Controlled Deposition of Electrospun Poly(Ethylene Oxide) Fibers. *Polymer (Guildf)* **2001**, *42*, 8163–8170, doi:10.1016/S0032-3861(01)00336-6.
75. Urbanek, O.; Sajkiewicz, P.; Pierini, F. The Effect of Polarity in the Electrospinning Process on PCL/Chitosan Nanofibres' Structure, Properties and Efficiency of Surface Modification. *Polymer (Guildf)* **2017**, *124*, 168–175, doi:10.1016/j.polymer.2017.07.064.
76. Csiszár, E.; Nagy, S. A Comparative Study on Cellulose Nanocrystals Extracted from Bleached Cotton and Flax and Used for Casting Films with Glycerol and Sorbitol Plasticisers. *Carbohydr Polym* **2017**, *174*, 740–749, doi:10.1016/j.carbpol.2017.06.103.
77. da Silva, D.P.B.; da Silva Moreira, L.K.; Cabral, I.B.; da Silva, C.N.S.; de Aleluia Batista, K.; Fajemiroye, J.O.; Costa, E.A. Chemistry, Biological Activities, and Uses of Cashew Gum. In *Gums, Resins and Latexes of Plant Origin: Chemistry, Biological Activities and Uses*; Murthy, H.N., Ed.; Springer International Publishing: Cham, 2022; pp. 291–305.
78. Bose, S.; Biswas, M. THE STRUCTURE OF THE GUM OF ANACARDIUM OCCIDENTALE. *Acta Hortic* **1985**, 207–217, doi:10.17660/ActaHortic.1985.108.37.
79. Yu, H.; Li, Y.; Li, T.; Chen, B.; Li, P.; Wu, Y. Fabrication of Aligned Eu(TTA)3phen/PS Fiber Bundles from High Molecular Weight Polymer Solution by Electrospinning. *Russian Journal of Physical Chemistry A* **2015**, *89*, 2455–2460, doi:10.1134/S003602441513018X/METRICS.

80. Silva, T.M.; Santiago, P.O.; Purcena, L.L.A.; Fernandes, K.F. Study of the Cashew Gum Polysaccharide for the Horseradish Peroxidase Immobilization — Structural Characteristics, Stability and Recovery. *Materials Science and Engineering: C* **2010**, *30*, 526–530, doi:10.1016/j.msec.2010.01.016.
81. Miranda, R.L. Cashew Tree Bark Secretion - Persectives for Its Use in Protein Isolation Strategies. *Open Glycosci* **2009**, *2*, 16–19, doi:10.2174/1875398100902010016.
82. de Paula, R.C.M.; Heatley, F.; Budd, P.M. Characterization of Anacardium Occidentale Exudate Polysaccharide. *Polym Int* **1998**, *45*, 27–35, doi:10.1002/(SICI)1097-0126(199801)45:1<27::AID-PI900>3.0.CO;2-9.
83. Anderson, D.M.W.; Bell, P.C. Structural Analysis of the Gum Polysaccharide from Anacardium Occidentale. *Anal Chim Acta* **1975**, *79*, 185–197, doi:10.1016/S0003-2670(00)89430-1.
84. Anderson, D.M.W.; Bell, P.C.; Millar, J.R.A. Composition of Gum Exudates from Anacardium Occidentale. *Phytochemistry* **1974**, *13*, 2189–2193, doi:10.1016/0031-9422(74)85026-0.
85. Vigani, B.; Rossi, S.; Milanesi, G.; Bonferoni, M.; Sandri, G.; Bruni, G.; Ferrari, F. Electrospun Alginate Fibers: Mixing of Two Different Poly(Ethylene Oxide) Grades to Improve Fiber Functional Properties. *Nanomaterials* **2018**, *8*, 971, doi:10.3390/nano8120971.
86. Martins, C.S.; Morgado, D.L.; Assi, O.B.G. Cashew Gum-Chitosan Blended Films: Spectral, Mechanical and Surface Wetting Evaluations. *Macromol Res* **2016**, *24*, 691–697, doi:10.1007/s13233-016-4103-8.
87. Lyu, H.; Sun, Z.; Liu, Y.; Yu, X.; Guo, C. Processing-Structure-Properties Relationships of Glycerol-Plasticized Silk Films. *Molecules* **2022**, *27*, 1339, doi:10.3390/molecules27041339.
88. Mohd Amin, A.M.; Mohd Sauid, S.; Musa, M.; Ku Hamid, K.H. THE EFFECT OF GLYCEROL CONTENT ON MECHANICAL PROPERTIES, SURFACE MORPHOLOGY AND WATER ABSORPTION OF THERMOPLASTIC FILMS FROM TACCA LEONTOPETALOIDES STARCH. *J Teknol* **2017**, *79*, 53–59, doi:10.11113/jt.v79.11327.
89. Basiak, E.; Lenart, A.; Debeaufort, F. How Glycerol and Water Contents Affect the Structural and Functional Properties of Starch-Based Edible Films. *Polymers (Basel)* **2018**, *10*, 412, doi:10.3390/polym10040412.
90. Farshi, P.; Salarian, R.; Rabiee, M.; Alizadeh, S.; Gholipourmalekabadi, M.; Ahmadi, S.; Rabiee, N. Design, Preparation, and Characterization of Silk Fibroin/Carboxymethyl Cellulose Wound Dressing for Skin Tissue Regeneration Applications. *Polym Eng Sci* **2022**, *62*, 2741–2749, doi:10.1002/pen.26057.
91. Nagakawa, Y.; Kato, M.; Suye, S.; Fujita, S. Fabrication of Tough, Anisotropic, Chemical-Crosslinker-Free Poly(Vinyl Alcohol) Nanofibrous Cryogels *via* Electrospinning. *RSC Adv* **2020**, *10*, 38045–38054, doi:10.1039/D0RA07322A.